ECCOMAS Congress 2016
VII European Congress on Computational Methods in Applied Sciences and Engineering
M. Papadrakakis, V. Papadopoulos, G. Stefanou, V. Plevris (eds.)
Crete Island, Greece, 5–10 June 2016

EULERIAN CALCULATIONS OF MULTIMATERIAL FLOWS WITH SUB-CELL RECONSTRUCTION OF INTERFACES

Igor S. Menshov[1,2] **and Pavel P. Zakharov**[2]

[1] Keldysh Institute for Applied Mathematics RAS
Miusskaya 4, 125047 Moscow Russia
e-mail: menshov@kiam.ru

[2] VNIIA ROSATOM
Sushchevskaya 22, 127055 Moscow Russia
jaquecostou@mail.ru

Keywords: multi-material fluid flow, interface capturing, composite Riemann problem, Godunov method

Abstract. *In the present paper we consider an Eulerian numerical method for calculating multi-material fluid. This method relates to the class of interface capturing methods that resolve material interfaces not exactly, but with some numerical smearing in space. To suppress this numerical smearing, we suggest a numerical flux approximation based on the sub-cell material interface reconstruction by simple patterns and the solution of the composite Riemann problem (CRP). It is found that the improved scheme captures the interface within one computational cell in 1D calculations. For multi-dimensional calculations we implement an approach of directional splitting that sufficiently decreases smearing of material interfaces what is demonstrated in computations of various multi-material applications.*

1 INTRODUCTION

The present paper is devoted to an Eulerian finite-volume method for numerical calculations of multimaterial fluid flows. We consider a heterogeneous medium that consists of different materials (components) separated with interfaces. Each component is described by its own EOS and governed by the system of compressible Euler equations. The mathematical model is applied that treats this multimaterial fluid flow as the flow of a heterogeneous multiphase fluid under the assumption of equilibrium in velocity, pressure, and temperature.

The method we develop belongs to the class of interface capturing methods. The interface is represented by the distribution in space of component mass fractions. The conventional Godunov method is applied for numerical flux approximation with exact or approximate Riemann solvers. This approach inevitably diffuses the interfaces between different materials because of the numerical viscosity that smears initially sharp distribution of mass fractions. The interface is given by a set of mixed cells occupied by the heterogeneous mixture of the components. As the calculation proceeds the domain of mixture cells expands involving more and more computational cells so that eventually the position of the interface in space is completely lost. This is the basic drawback of the conventional Godunov method.

Another drawback appears when we try to compute flows of condensed and gaseous materials with rarefaction waves. The EOSs in this case are quite different and admit different regions of admissible values of thermodynamic parameters. Solids admit negative pressure while the gaseous phase not. Because of the equilibrium assumption the pressure in mixed cells should be always positive. This leads to an artificial numerical effect that we name as pseudo-fracture. It shows up in the formation of a small region of mixed cells near the pure solid region where the solid volume fraction drastically decreases [1].

In order to fix these drawbacks one can sharpen smearing interfaces by implementing some techniques commonly referred to as anti-diffusive [2-3]. We suggest an alternative way that is based on a numerical flux approximation that takes into account the interface local position or in other words the material sub-cell structure in mixed cells. Following this way we come to generalized formulation of the Riemann problem for the medium that contains two materials separated with the interface. This formulation includes an initial discontinuity in one component and also the contact point of the interface [4]. We refer this problem as Composite Riemann Problem (CRP). The solution of the CRP provides more accurate approximation of the numerical flux in mixed cells. Various numerical results demonstrate that the CRP technique allows us to reduce the mixed zone to only one computational cell in 1D calculations and to a few cells in multidimensional calculations.

2 MODELING MULTI-MATERIAL FLOWS

We consider a heterogeneous multi-material compressible medium that in general consists of N components (materials). We assume that each component is thermodynamically a two-parameter medium and is governed by mechanical and thermal EOSs in the form of functional relations between density ρ_i^o, pressure p_i, specific internal energy e_i, and temperature T_i as $e_i = e_i(\rho_i^o, p_i)$ and $T_i = T_i(\rho_i^o, p_i)$, respectively. Here, $i = 1, \ldots, N$ indicates the index of the component. The mathematical model of the multi-phase medium with velocity, pressure, and temperature equilibrium, so called the PT model,

$$\mathbf{v} = \mathbf{v}_1 = \ldots = \mathbf{v}_N,\ p = p_1 = \ldots = p_N,\ T = T_1 = \ldots = T_N, \tag{1}$$

with the assumption of additivity of internal energies is used to describe the multi-material fluid flow [18]. The governing equations of this model can be written in the conservative form as follows:

$$\frac{\partial \mathbf{q}}{\partial t} + \frac{\partial \mathbf{f}_1}{\partial x} + \frac{\partial \mathbf{f}_2}{\partial y} + \frac{\partial \mathbf{f}_3}{\partial z} = 0\,, \tag{2}$$

where $\mathbf{q}$ is the vector of conservative variables, and $\mathbf{f}_1$, $\mathbf{f}_2$, and $\mathbf{f}_3$ are the flux vectors along the x-axis, y-axis, and z-axis, respectively:

$$\mathbf{q} = \begin{pmatrix} \rho \\ \rho v_1 \\ \rho v_2 \\ \rho v_3 \\ \rho E \\ \rho\beta_1 \\ \dots \\ \rho\beta_N \end{pmatrix},\ \mathbf{f}_1 = \begin{pmatrix} \rho v_1 \\ \rho v_1 v_1 + p \\ \rho v_1 v_2 \\ \rho v_1 v_3 \\ v_1(\rho E + p) \\ \rho v_1 \beta_1 \\ \dots \\ \rho v_1 \beta_N \end{pmatrix},\ \mathbf{f}_2 = \begin{pmatrix} \rho v_2 \\ \rho v_2 v_1 \\ \rho v_2 v_2 + p \\ \rho v_2 v_3 \\ v_2(\rho E + p) \\ \rho v_2 \beta_1 \\ \dots \\ \rho v_2 \beta_N \end{pmatrix},\ \mathbf{f}_1 = \begin{pmatrix} \rho v_3 \\ \rho v_3 v_1 \\ \rho v_3 v_2 \\ \rho v_3 v_3 + p \\ v_3(\rho E + p) \\ \rho v_3 \beta_1 \\ \dots \\ \rho v_3 \beta_N \end{pmatrix}. \tag{3}$$

Here, ρ is the mixture density, $\rho = \sum_{i=1}^{N} \alpha_i \rho_i^o$, $\beta_i = \alpha_i \rho_i^o / \rho$; α_i, β_i are the volume and the mass fractions of i-th component, respectively, $\mathbf{v} = (v_1, v_2, v_3)^{\mathrm{T}}$ is the velocity vector in Cartesian coordinates, $E = e + 0.5\mathbf{v}^2$ is the mixture specific total energy, $e = \sum_{i=1}^{N} \beta_i e_i$ is the mixture specific internal energy. Along with the vector of conservative variables $\mathbf{q}$, we shall also consider the vector of primitive variables $\mathbf{z} = (\rho, v_1, v_2, v_3, p, \beta_1, \dots, \beta_N)^{\mathrm{T}}$.

The system of equations (2) and (3) is closed by mixture EOSs that are derived from the assumption of pressure and temperature equilibrium:

$$e = \sum_{i=1}^{N} \beta_i e_i(\rho_i^o, p_i) = \sum_{i=1}^{N} \beta_i e_i(p_i, T_i) = e(p, T, \beta_1, \dots, \beta_N)\,, \tag{4}$$

$$1 = \sum_{i=1}^{N} \alpha_i = \rho \sum_{i=1}^{N} \frac{\beta_i}{\rho_i^o(p_i, T_i)} = \rho \sum_{i=1}^{N} \frac{\beta_i}{\rho_i^o(p, T)}\,. \tag{5}$$

The multi-material fluid flow model can be considered as the multiphase model with a particular distribution of mass fractions given by

$$\beta_i(\mathbf{r}) = 1,\ \beta_j(\mathbf{r}) = 0,\ \forall j \neq i,\ \mathbf{r} = (x, y, z) \in \Omega_i(t),\ i = 1, \dots, N. \tag{6}$$

If the number of materials N is equal to one, Equations (2) and (3) reduce to the standard Euler equations for a single-material fluid flow.

If the mixture is characterized at initial ($t = 0$) by a distribution of type (6), then the same type of distribution is theoretically kept for $t > 0$, and two or more different components are never at the same point of space. However, this is not the case in numerical simulations.

When an Eulerian approach is employed, the captured material interface is found to be a region of mix cells, separating sub-domains of a pure fluid flows. The width of this region depends on the numerical scheme to be used and can span from a few to dozens of grid cells. A challenging problem in this approach is to reduce the width of numerical interface smearing as much as possible. As a solution to this problem, one can apply high-order numerical schemes or so-called anti-diffusive techniques. We suggest an alternative method to cope with numerical smearing of material interfaces, which is based on a special procedure of resolving materials at the sub-cell level.

3 THE DISCRETE MODEL

The spatial discretization of Equations (2) and (3) is performed with the finite volume method. With the explicit time marching scheme, this results in the following system of discrete equations:

$$\mathbf{q}_i^{n+1} = \mathbf{q}_i^n - \frac{\Delta t}{V_i} \sum_\sigma T_\sigma^{-1} \mathbf{F}_\sigma S_\sigma \,. \tag{7}$$

where the subscripts i and σ denote the cell and its face, respectively, V_i is the volume of the i-th cell, S_σ is the face area, $\mathbf{T}$ is the transforming matrix from the absolute system of coordinates to a coordinate system associated with the face. The vector $\mathbf{F} = \mathbf{F}(\mathbf{Q})$, $\mathbf{Q} = \mathbf{Tq}$, has the form of a locally 1D flux in the direction of the outward face normal

$$\mathbf{F} = \mathbf{F}(\mathbf{Q}) = \left(\rho v_n, \rho v_n^{\,2} + p, \rho v_n v_k, \rho v_n v_l, \rho v_n E + p v_n, \rho v_n \beta_1, \ \ldots\ , \rho v_n \beta_N\right)^T , \tag{8}$$

where the subscripts n, k, and l indicate normal and tangential components of the velocity vector.

In the conventional Godunov method the numerical flux $\mathbf{F}_\sigma$ is calculated as follows:

$$\mathbf{F}_\sigma = \mathbf{F}\left(\mathbf{Q}^{RP}\left(\mathbf{Z}_i^\sigma, \mathbf{Z}_{\sigma(i)}^\sigma\right)\right) = \mathbf{F}\left(\mathbf{Q}^{RP}\left(\mathbf{Tz}_i^\sigma, \mathbf{Tz}_{\sigma(i)}^\sigma\right)\right) \tag{9}$$

where $\mathbf{Q}^{RP}$ denotes the exact solution to the Riemann problem at the line $x = 0$ with initial data $\mathbf{Z}_i^\sigma$ and $\mathbf{Z}_{\sigma(i)}^\sigma$ on the left and on the right of the initial discontinuity, respectively. The vector $\mathbf{z}$ is the primitive vector. The superscript σ indicates that these values are taken at the cell face depending of the scheme order of accuracy.

In the case of single-material fluid flow, the numerical flux can be also calculated by means of an approximate Riemann solver as Rusanov method [5], HLL [6] and others. These flux approximations can be applied straightforwardly to solve multi-material fluid flow modeled by Equations (2) and (3). Thus, calculations in the whole domain can be executed in the same manner, both in pure and mix cells. We refer this straightforward extension of the conventional numerical flux approximation to the multi-material case as a *standard flux approximation*.

The usage of the standard flux approximations results in significant numerical smearing of material interfaces. These approximations do not regard the presence of the sharp material interface inside mix cells. Thus, if a non-zero mass flux appears from a mix cell to an adjacent pure cell it inevitably would result in non-zero mass fluxes of all components containing in the mix cell.

As a solution to this problem, we suggest modifications for the numerical flux approximation for those cell faces that border at least one mix cell. These modifications are made on the base of the sub-cell material interface reconstruction and the CRP solution. We call this

flux approximation a *CRP-based flux approximation.* If no mix cell borders the face, numerical flux is calculated by one of standard flux approximations.

3.1 The CRP-based flux approximation

In order to introduce the modifications of the flux approximation for the cell faces bordering at least one mix cell, we have to consider two possible situations when one cell is pure and another is mixed or both are mixed. For clarity, let the pure cell is filled with the material "A", and the mix cell is filled with the materials "A" and "B".

If the connectivity at a cell face σ is of the type "mix-pure", we assume that the contact surface between materials "A" and "B" in the mix cell is parallel to the face σ and located at a distance δ, and material "A" in the mix cell borders the material "A" in the pure cell. The distance $\delta = \alpha_A V/S_\sigma$, where α_A is the material "A" volume fraction in the mix cell, V is the mix cell volume and S_σ is the face σ area.

For a given mixture state vector $\mathbf{z} = (\rho, \mathbf{v}, p, \beta_A, \beta_B)^T$ we can derive vectors $\mathbf{z}_A$ and $\mathbf{z}_B$, characterizing the state of materials "A" and "B" in the mix cell: $\mathbf{z}_A = (\rho^o{}_A, \mathbf{v}, p, 1, 0)^T$ and $\mathbf{z}_B = (\rho^o{}_B, \mathbf{v}, p, 0, 1)^T$, with $\rho^o{}_{A/B} = \rho^o{}_{A/B}(p, T)$ being material densities defined with the corresponding EOSs. The material densities are related with volume fractions $\alpha_{A/B}$, $\alpha_{A/B} = \rho\beta_{A/B}/\rho^o{}_{A/B}$. Thus, the position of the material interface in the mix cell is uniquely located. Note that in 1D such a reconstruction of the interface is natural.

Applying the interface reconstruction in the mix cell, we then calculate the numerical flux $\mathbf{F}_\sigma$ at the face σ by means of the CRP solution with the proper initial data $\mathbf{Z}_B^{(L)}, \mathbf{Z}_A^{(L)}, \mathbf{Z}_A^{(R)}$ as follows:

$$\mathbf{F}_\sigma = \mathbf{F}^{CRP}\left(\mathbf{Z}_B^{(L)}, \mathbf{Z}_A^{(L)}, \mathbf{Z}_A^{(R)}, \delta\right) \tag{10}$$

where the superscripts (L) and (R) indicate the left and right cells, respectively. It is obviously that we can define the term $\mathbf{F}^{CRP}\left(\mathbf{Z}_B^{(L)}, \mathbf{Z}_A^{(L)}, \mathbf{Z}_A^{(R)}, \delta\right)$ for $\delta = 0$ ($\alpha_A = 0$) as

$$\mathbf{F}^{CRP}\left(\mathbf{Z}_B^{(L)}, \mathbf{Z}_A^{(L)}, \mathbf{Z}_A^{(R)}, 0\right) = \mathbf{F}\left(\mathbf{Q}^{RP}\left(\mathbf{Z}_B^{(L)}, \mathbf{Z}_A^{(R)}\right)\right), \tag{11}$$

and for $\delta = h = V/S_\sigma$ ($\alpha_A = 1$) as

$$\mathbf{F}^{CRP}\left(\mathbf{Z}_B^{(L)}, \mathbf{Z}_A^{(L)}, \mathbf{Z}_A^{(R)}, h\right) = \mathbf{F}\left(\mathbf{Q}^{RP}\left(\mathbf{Z}_A^{(L)}, \mathbf{Z}_A^{(R)}\right)\right). \tag{12}$$

Details of the CRP solver are given can be found in [1].

If the connectivity at a cell face σ is of the type "mix-mix", a reasonable assumption is that the contact surface should in a some way cross the cell face σ, passing through the mix cells. Following the procedure mentioned above, one can calculate component vectors $\mathbf{z}_{A/B}$ and volume fractions $\alpha_{A/B}$ for each cell and then reconstruct contact surface in the cells as shown in Figure 1b. In general, reconstructed contact surfaces do not match at the cell face ($\alpha_A^{(L)} < \alpha_A^{(R)} < 0.5$). One can suggest patterns for the sub-cell interface reconstruction with continuous behavior of the contact surface at the face σ. We assume that the contact surface crosses the face in an intermediate point between points "1" and "2" as shown in Figure 1c.

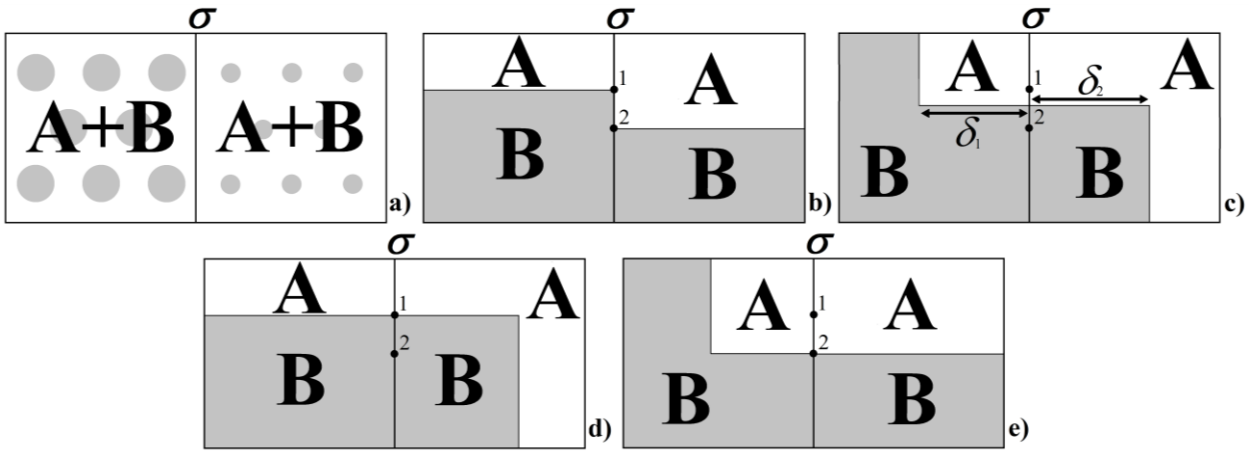

Figure 1. Patterns for the sub-cell interface reconstruction in the case of "mix-mix " cell connectivity.

For the patterns of Figure 1c-1e, we can calculate the numerical flux as a linear combination of two fluxes defined on corresponding CRP solutions as follows:

$$\mathbf{F}_\sigma = \tilde{\alpha}\mathbf{F}^{CRP}\left(\mathbf{Z}_{\mathrm{B}}^{(\mathrm{L})}, \mathbf{Z}_{\mathrm{A}}^{(\mathrm{L})}, \mathbf{Z}_{\mathrm{A}}^{(\mathrm{R})}, \delta_1\right) - (1-\tilde{\alpha})\mathbf{F}^{CRP}\left(\mathbf{Z}_{\mathrm{A}}^{(\mathrm{R})}, \mathbf{Z}_{\mathrm{B}}^{(\mathrm{R})}, \mathbf{Z}_{\mathrm{B}}^{(\mathrm{L})}, \delta_2\right), \tag{13}$$

where $\tilde{\alpha} = w\alpha_{\mathrm{A}}^{(\mathrm{L})} + (1-w)\alpha_{\mathrm{A}}^{(\mathrm{R})}$, $w \in [0, 1]$. The parameter w defines the intermediate point in Figure 1c. Thus, the numerical flux across a face σ is calculated by means of solving one or two appropriate CRPs.

It should be noted that the interface reconstruction with local 1D patterns is not a real one. It is implemented independently for each cell face on the base of only volume fraction values in mix cells bordering the considered face. This results in a very simple algorithm. However, it has certain drawbacks that are a penalty of these simplifications. We discuss this issue in section of numerical results. In order to overcome these drawbacks, we implement a method with the directional splitting technique which allows to better utilize a 1D nature of the proposed flux approximation.

An open issue is the choice of w in Equation (13) when a "mix-mix" pattern is used. In that case the sub-cell interface reconstruction can be done uniquely just on the base of volume fractions. Most calculations presented in this paper are done with $w = 0$ that corresponds to a "mix-mix" pattern of Figure 1e. In some cases we use also values $w = 0.5$ and $w = 1$. Anyway, the parameter is used as constant in the calculations. A dynamical approach where it is evaluated depending on local distributions of mass and volume fractions is the purpose of our future research.

3.2 The scheme with splitting in directions

The sub-cell interface reconstruction of the previous subsection is by nature locally one-dimensional and carried out independently for all cell faces. To adapt this approach to multi-dimensional calculations, we develop also its implementation based on the method of splitting in directions. In the case of Cartesian grids the explicit time integration numerical scheme is written as

$$\mathbf{q}_i^{n+1} = \mathbf{q}_i^n - \frac{\Delta t}{V_i}(\mathbf{F}_{1x} + \mathbf{F}_{2x} + \mathbf{F}_{1y} + \mathbf{F}_{2y}), \tag{14}$$

where $\mathbf{F}_{1x}$, $\mathbf{F}_{2x}$ and $\mathbf{F}_{1y}$, $\mathbf{F}_{2y}$ are numerical fluxes along the x-axis and the y-axis, respectively. For certainty, we consider the 2D case here.

A directionally splitted scheme can be written as follows:

$$\mathbf{q}_i^{nx} = \mathbf{q}_i^n - \frac{\Delta t}{V_i}(\mathbf{F}_{1x} + \mathbf{F}_{2x}), \mathbf{q}_i^{n+1} = \mathbf{q}_i^{nx} - \frac{\Delta t}{V_i}(\mathbf{F}_{1y} + \mathbf{F}_{2y}), \tag{15}$$

where the fluxes $\mathbf{F}_{1x}$ and $\mathbf{F}_{2x}$ are calculated with values of the n-th time layer $\{\mathbf{q}^n\}$, and the fluxes $\mathbf{F}_{1y}$ and $\mathbf{F}_{2y}$ are calculated with those of the nx-th time layer $\{\mathbf{q}^{nx}\}$.

4 NUMERICAL RESULTS

In our previous paper [1], numerical examples mostly concerned one-dimensional problems. It was shown that CRP-based flux approximation always allows to capture the interface within just one computational cell. In the 1D case there should not be two neighboring mix cells and only a "mix-pure" pattern for the sub-cell interface reconstruction can exist. This is not the case in 2D calculations. We have to use "mix-mix" pattern for the sub-cell interface reconstruction shown in Figure 2c, which is not so definite procedure as in the case of "mix-pure" cell connectivity. In this section we present numerical results of calculations with various implementations of the "mix-mix" interface reconstruction and discuss their interface capturing properties.

4.1 The problem of shock/contact interaction

The problem statement is sketched in Figure 2. At initial the lead-gas interface has a triangle disturbance with the depth of 0.0035 cm. The computational domain is $0 \le x \le 1.6$ cm, $0 \le y \le 0.2$ cm occupied by a lead sample with a length of 0.5 cm and a gas. Boundary conditions are following: a rigid wall boundary condition is imposed at $x = 0$, $y = 0$, $y = 0.2$ cm and a non-reflecting boundary condition is imposed at $x = 1.6$ cm. The computational grid consists of 800 and 100 along the x-axis and the y-axis, respectively. The CFL number is equal to 0.5.

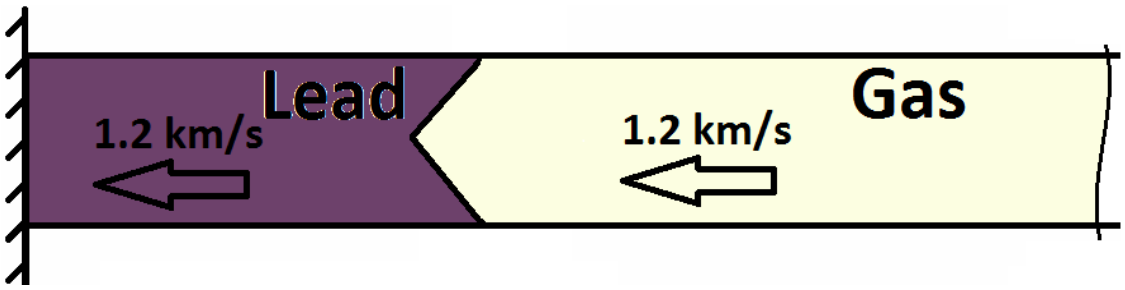

Figure 2. A sketch of the shock/contact interaction problem.

To highlight the importance of keeping the interface region as small as possible, calculations of this problem are carried out with the first order of accuracy using Rusanov and CRP-based flux approximation. In the CRP-based calculation we use the directional splitting technique and a "mix-mix" pattern of Figure 1e.

As can be seen from Figure 3, the Rusanov flux calculation results in a numerical effect of pseudo-fracturing in lead (a narrow region of small density near the interface). The jet formation is found to be underestimated (see Figure 3). Figure 4 shows the jet formation in the CRP-based flux calculation with no any pseudo-fracture in lead. The comparison of the

cell type distribution for both calculations at a time moment t = 7.25 μs is presented in Figure 5. Black color indicates mix cells, white and grey colors indicate pure gas cells and pure lead cells, respectively. We can observe that the lead-gas interface is captured within few computational cells in the CRP-based flux calculation, while it turns to be an expanded domain in the Rusanov flux calculation.

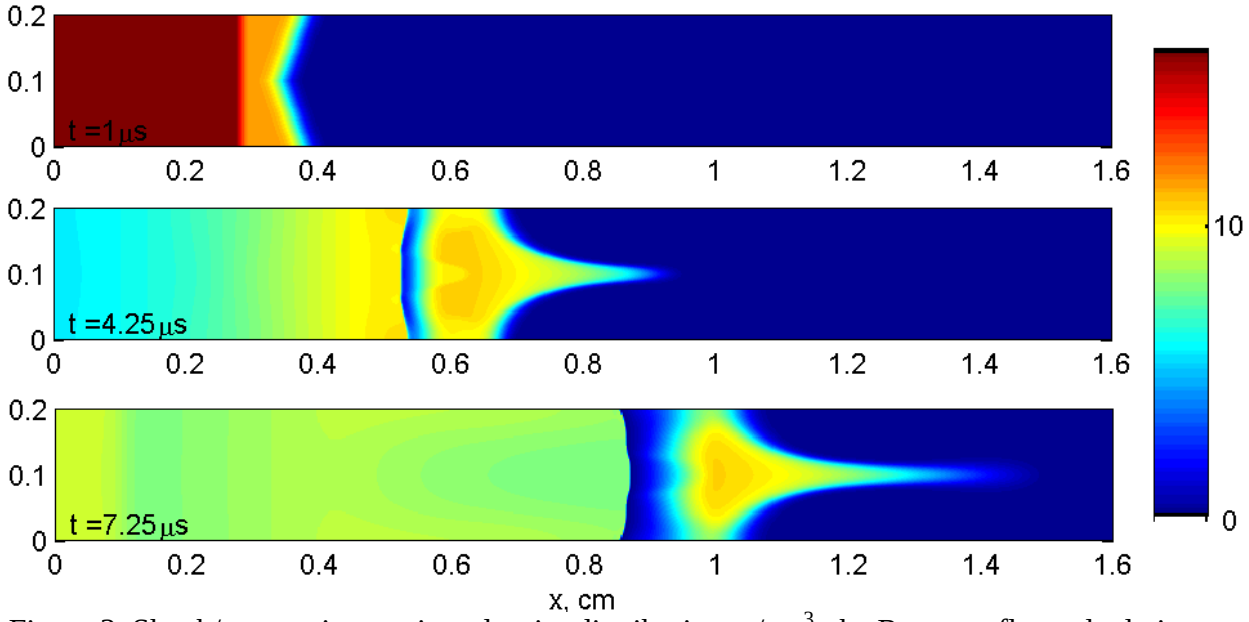

Figure 3. Shock/contact interaction: density distribution, g/cm^3, the Rusanov flux calculation.

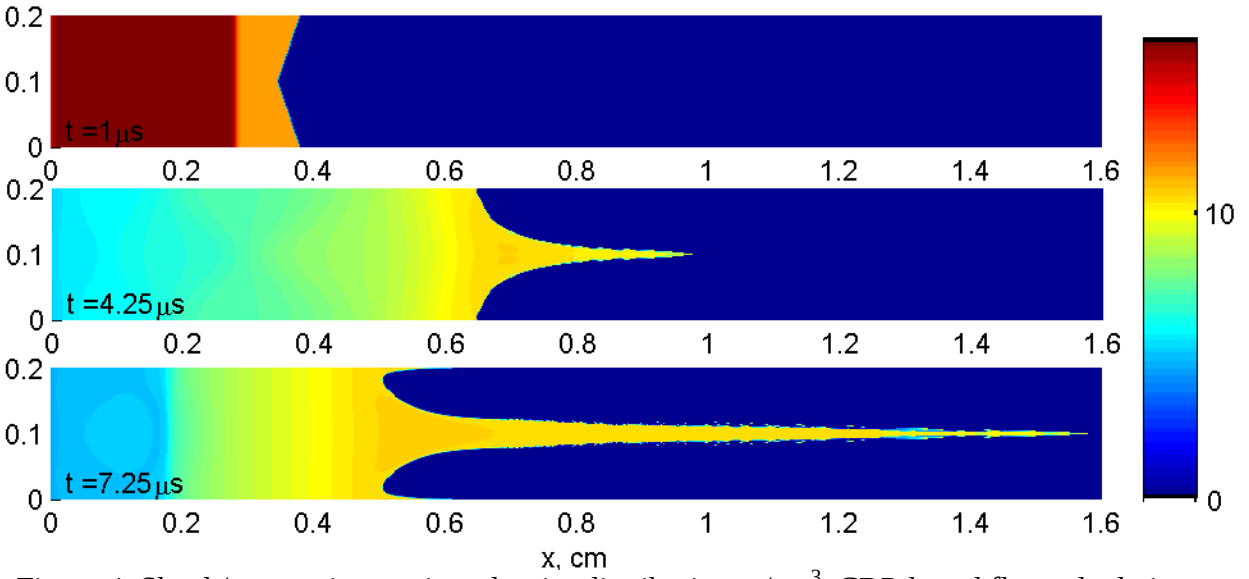

Figure 4. Shock/contact interaction: density distribution, g/cm^3, CRP-based flux calculation.

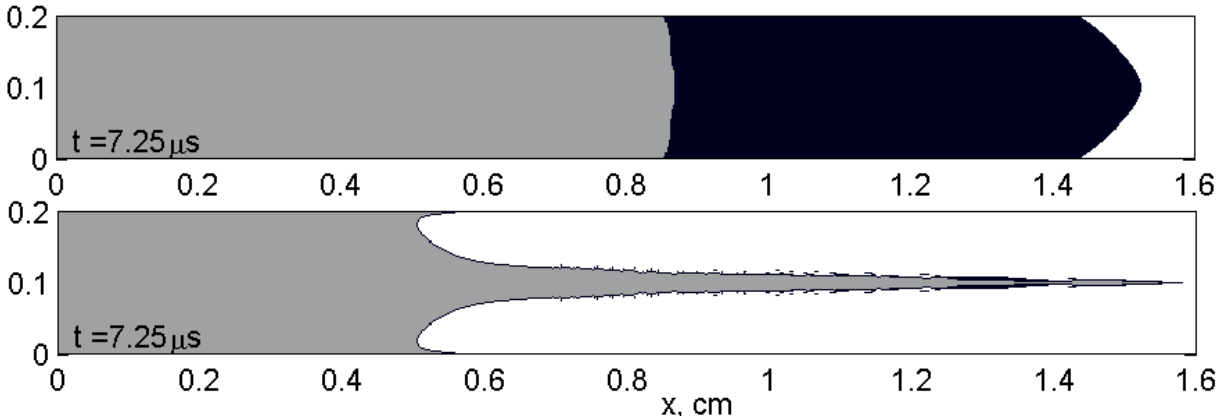

Figure 5. Shock/contact interaction: cell type distribution,
the Rusanov flux (top) and the CRP-based flux (lower), t = 7.25 μs.

4.2 The problem of underwater air bubble collapse

The problem statement is the same as in [7]. The computational domain is $0 \le x \le 1.2$ cm, $0 \le y \le 1.2$ cm. The air bubble diameter is 0.6 cm, and its center is at (0.6, 0.6) cm. The EOS of air and water is taken in the form of a stiffened gas EOS. Periodical boundary conditions are imposed on the bottom and top boundary of the computational domain. The computational grid consists 200 of computational cells in each direction. The CFL number is equal to 0.5.

Figure 6 shows the cell type distributions at a time moment t = 3.25 μs for six variants of calculation. Black color indicates mix cells, white and grey colors indicate pure air cells and pure water cells, respectively. The top row of figures corresponds to calculations with the directional splitting off. The lower row corresponds to calculation with directional splitting. The left column corresponds to a "mix-mix" pattern of Figure 1c with w = 0.5, the middle column - a "mix-mix" pattern of Figure 1d and the right column - a "mix-mix" pattern of Figure 1e.

One can conclude from Figure 6 that the directional splitting technique improves interface capturing properties. It can be also observed that different "mix-mix" patterns for the sub-cell interface reconstruction result in different forms of numerical smearing, especially in the case of non splitting calculations.

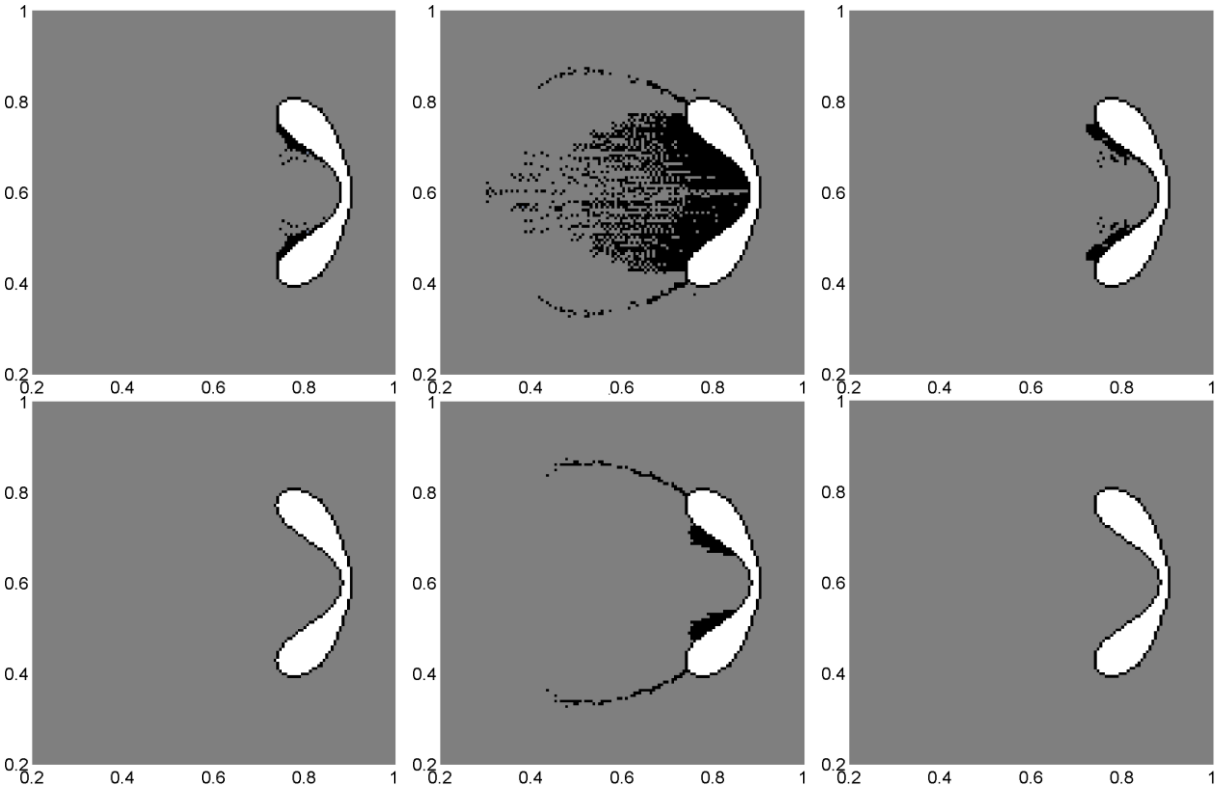

Figure 6. The underwater air bubble collapse: the cell type distribution at t = 3.25 μs. The comparison of different "mix-mix" patterns and directional splitting.

Figure 7 shows results of calculations with the CRP-based flux on a fine grid consisting of 2000 computational cells in each direction. Such a grid resolution allows to capture the formation of small scale secondary jets. One can see a narrow water jet that slits the bubble and hits the water from the base. These calculations have been performed with the directional splitting, a "mix-mix" pattern of Figure 1e in the sub-cell interface reconstruction, and the second order of accuracy.

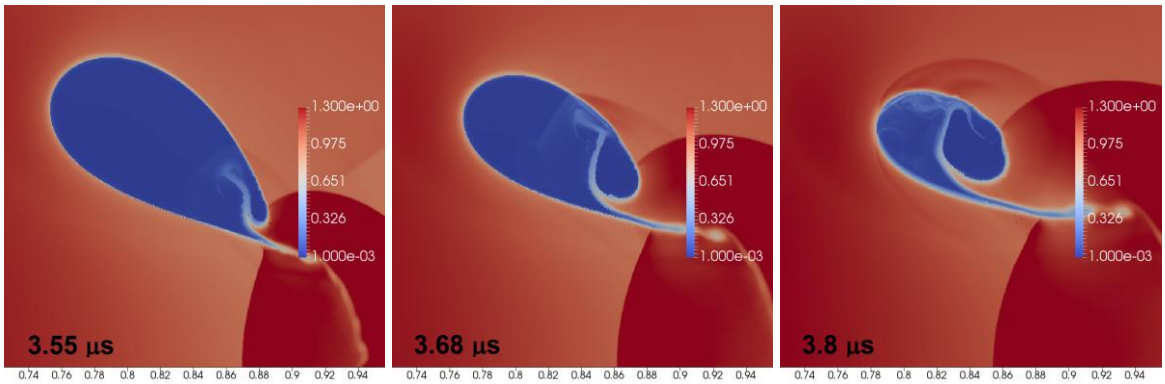

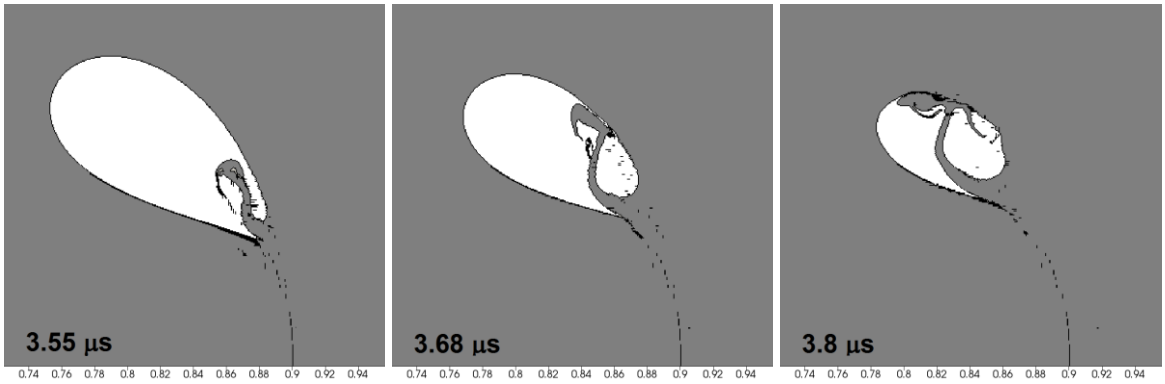

Figure 7. The underwater air bubble collapse: the formation of secondary jets.
The density distribution, g/cm^3 (top) and the cell type distribution (low).

4.3 The triple point problem

The problem statement is taken from [8]. The computational domain is $0 \le x \le 7$ and $0 \le y \le 3$. The first sub-domain ($0 \le x \le 1$, $0 \le y \le 3$) contains a high-pressure high-density material. The second sub-domain ($1 < x \le 7$, $0 \le y < 1.5$) contains a low-pressure high-density material. The third sub-domain ($1< x \le 7$, $1.5 \le y \le 3$) a low-pressure low-density material. All three materials are governed by the ideal gas EOS. The rigid wall condition is imposed at all boundaries of the computational domain. We solve this problem as a two-material problem and do not distinguish materials in the first and the third sub-domain.

Figure 8 shows results with the directional splitting, a "mix-mix" pattern of Figure 1e, and the second order of accuracy on a computational grid of 4200 and 1800 cells along the x-axis and the y-axis, respectively. The CFL number is equal to 0.5. One can observe that the material interface undergoes a Kelvin-Helmholtz instability that results in a large deformation of the interface with the formation of small-scale jet-like structures.

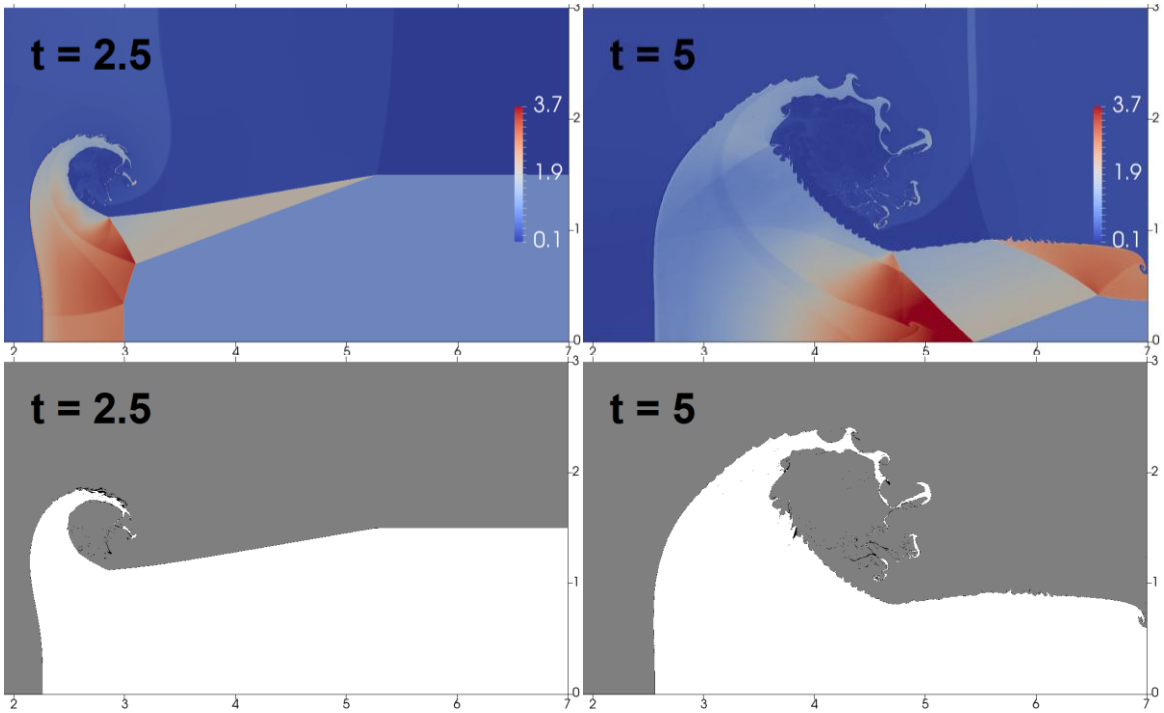

Figure 8. The triple point problem: the formation of Kelvin-Helmholtz instability.
The density distribution, g/cm^3 (top) and the cell type distribution (low).

5 CONCLUSIONS

An Eulerian finite-volume method for multi-material fluid flows modeled by a multiphase medium with pressure, temperature and velocity equilibrium is discussed. The method belongs to the class of interface capturing approaches and aims to reduce numerical smearing of material interfaces. To achieve this goal, we have introduced the sub-cell interface reconstruction procedure based on simple interfaces patterns. The proposed sub-cell interface structure is taken into account in calculating the numerical flux across a cell face bordering a mix cell. This is performed with a proper IVP - a Composite Riemann Problem (CRP) that involves both a point of initial discontinuity and a material contact point. The numerical flux approximation based on this CRP solution strongly reduces the interface smearing region. Numerical experiments have shown the reduction of the interface region up to a few computational cells in 2D tests.

The work reported in this paper was partially supported by the grant No 14-11-00872 from the Russian Scientific Fund.

REFERENCES

[1] I.S. Menshov, P.P. Zakharov. On the composite Riemann problem for multimaterial fluid flows. *International Journal for Numerical Methods in Fluids*, **76**(2), 109-127, 2014.

[2] T. Nonomura, K. Kitamura, K. Fujii. A simple interface sharpening technique with a hyperbolic tangent function applied to compressible two-fluid modeling. *Journal of Computational Physics,* **258,** 95–117, 2014.

[3] K.K. So, X.Y. Hu, N.A. Adams. Anti-diffusion interface sharpening technique for two-phase compressible flow simulations. *Journal of Computational Physics,* **231(11),** 4304–4323, 2012.

[4] I. Menshov and P. Zakharov. A Composite Riemann Solver for Improving Interface Capturing in Multimaterial Calculations. *MULTIMAT 2015*, Wurzburg, Germany, September 7 - 11, 2015.

[5] V.V. Rusanov. Calculation of Interaction of Non-Steady Shock Waves with Obstacles. *USSR Computational Mathematics and Mathematical Physics*, **1(2)**, 267-279, 1961.

[6] A . Harten, P.D. Lax, and B . Van Leer. On upstream differencing and Godunov-type schemes for hyperbolic conservation laws. *SIAM Review*, **25(1),** 35-61, 1983.

[7] R.R. Nourgaliev, T.N. Dinh, T.G. Theofanous. Adaptive characteristics-based matching for compressible multifluid dynamics. *Journal of Computational Physics,* **213(2),** 500–529, 2006.

[8] M. Kucharik, R.V. Garimella, S.P. Schofield, M.J. Shashkov . A comparative study of interface reconstruction methods for multi-material ALE simulations. *Journal of Computational Physics.,* **229(7),** 2432-2452, 2010.